

Conditioning diffusion models by explicit forward-backward bridging

Adrien Corenflos*

Aalto University University of Warwick
adrien.corenflos@warwick.ac.uk

Zheng Zhao*

Uppsala University
zheng.zhao@it.uu.se

Simo Särkkä

Aalto University

Jens Sjölund

Uppsala University

Thomas B. Schön

Uppsala University

Abstract

Given an unconditional diffusion model $\pi(x, y)$, using it to perform conditional simulation $\pi(x | y)$ is still largely an open question and is typically achieved by learning conditional drifts to the denoising SDE after the fact. In this work, we express conditional simulation as an inference problem on an augmented space corresponding to a partial SDE bridge. This perspective allows us to implement efficient and principled particle Gibbs and pseudo-marginal samplers marginally targeting the conditional distribution $\pi(x | y)$. Contrary to existing methodology, our methods do not introduce any additional approximation to the unconditional diffusion model aside from the Monte Carlo error. We showcase the benefits and drawbacks of our approach on a series of synthetic and real data examples.

1 Introduction

Denoising diffusion models (Song et al., 2021; Ho et al., 2020) have recently received a lot of attention as general-purpose samplers for generative modelling in diverse fields such as image analysis (Luo et al., 2023), protein folding (Wu et al., 2023), and statistical inference (Vargas et al., 2023). At the core, given a target distribution π_0 that we want to generate samples from, and a time-homogeneous stochastic differential equation (SDE, see, e.g., Karatzas and Shreve, 1991)

$$dX_t = f(X_t) dt + dW_t, \quad X_0 \sim \pi_0, \quad (1)$$

with stationary distribution π_{ref} , they sample from π_0 by “denoising” (1) via Doob’s h -transform (Rogers and Williams, 2000). Formally, let π_t be the distribution of X_t under (1), and assume that we know how to sample from π_T for some $T > 0$. We can obtain approximate samples from π_0 by sampling from

$$dU_t = f_{\text{rev}}(U_t, t) dt + dB_t, \quad U_0 \sim \pi_T, \quad (2)$$

where B is another Brownian motion, and we write $f_{\text{rev}}(U_t, t) := -f(U_t) + \nabla \log \pi_{T-t}(U_t)$. When $T \gg 1$, and under ergodicity guarantees (Meyn and Tweedie, 2009), $\pi_T \approx \pi_{\text{ref}}$. Consequently, if (1) is chosen such that π_{ref} is easy to sample from, then the only remaining difficulty is computing the score $\nabla \log \pi_{T-t}$, which is typically overcome by training a neural network to approximate the score function (or drift) via score matching (Hyvärinen, 2005).

Once the score function has been computed, approximate samples from π can be obtained by running a discretised simulation of (2)

$$\begin{aligned} U_k &= U_{k-1} - (t_k - t_{k-1}) f_{\text{rev}}(U_{k-1}, t_{k-1}) + \sqrt{t_k - t_{k-1}} Z_k, \\ U_0 &\sim \pi_{\text{ref}}, \quad Z_k \sim \mathcal{N}(0, I_d), \end{aligned} \quad (3)$$

*Equal authorship

for an integration grid $0 = t_0 < t_1 < \dots < t_K = T$, where I_d is a d -dimensional diagonal matrix.

A typical choice for the forward SDE (1) is a Langevin diffusion targeting a standard Gaussian distribution, namely taking $f(x) = -x$, also known as the Ornstein–Uhlenbeck process. Variants of this choice have been proposed, such as the use of time-dependent diffusion coefficient (Song and Ermon, 2020) or non-Markovian dynamics (Song et al., 2020). A remarkable extension is the use of Schrödinger bridges (De Bortoli et al., 2021), which generalise the approach by forming SDE bridges between two arbitrary distributions, thereby allowing for the generation of samples from π_0 given samples from $\pi_T = \pi_{\text{ref}}$, in finite time rather than asymptotically as $T \gg 1$ at the cost of learning both the forward and backward dynamics.

1.1 Problem formulation

Despite their success, using diffusion models to perform *exact* conditional simulation is still largely an open question, whereby the goal is to sample from the conditional distribution $\pi(x | y)$. Here, x represents the sample of interest, unconditionally obtained from the diffusion model (3) and y is a conditioning variable. In this article, we consider the problem of exact conditioning *within* diffusion models. This is a question posed by Bayesian inference in general (Martin et al., 2023), also known as *inpainting* and *super-resolution* within the computer vision community.

We assume that a diffusion model (e.g., Schrödinger bridge) has been trained to sample from the joint distribution $\pi(x, y)$, and our aim is to produce (asymptotically) exact samples from the conditional distribution $\pi(x | y)$ on top of the trained model.

1.2 Contributions

We propose a new Markov chain Monte Carlo (MCMC, Meyn and Tweedie, 2009) method for conditioning *within* diffusion models, to obtain samples from $\pi(x | y)$. Our method, which we call forward-backward bridging (FBB), is based on the following observation: conditioning a diffusion model can be written as a partial SDE bridge, constructed by running a preliminary forward simulation, noising the initial states (X_0, y) into (X_T, Y_T) , and then a backward particle filter corresponding to bridging back to the target distribution $\pi_0(x | y)$. This perspective was originally proposed in Trippe et al. (2023) and in the work, developed independently from ours, of Dou and Song (2024).

In contrast to both these works, here we take a more principled approach of treating the conditioning problem as an inference problem on the joint $p(x_0, x_T, y_T | Y_0 = y)$, as well as all intermediary missing steps. We achieve this by leveraging the dynamic structure of diffusion models and alternating between a forward noising process and a conditional sequential Monte Carlo (CSMC, Andrieu et al., 2010) algorithm, thereby forming a Gibbs sampler (Geman and Geman, 1984) alternatively sampling from the joint and conditional distributions of the diffusion model. This presents the substantial benefits of correcting the sampler for lack of ergodicity (i.e., the fact of using finite number of particles, and that $T < \infty$ being finite create biases in Trippe et al., 2023; Dou and Song, 2024) as well as providing a way to treat Schrödinger bridge samplers (De Bortoli et al., 2021; Shi et al., 2023) which cannot be handled by existing methodology.

The contributions of this article are therefore as follows:

1. We develop forward-backward bridging (FBB), a new particle Gibbs (Andrieu et al., 2010) method for conditioning diffusion models.
2. In Section 3, we show how, when the noising process is tractable and separable, which is the case for the usual denoising diffusion models, the method can be adapted to be run in-place, at zero memory cost using a pseudo-marginal approach (Andrieu et al., 2010). This provides a principled and unbiased generalisation of Trippe et al. (2023).
3. The benefits of our approach are illustrated in Section 4 on a series of high-dimensional benchmarks, showcasing the improved sample quality.

2 Forward-backward conditioning of diffusions

Let us consider a target density $\pi(x, y) = \pi(y) \pi(x | y)$ for which we have a diffusion sampler, and a value y for conditioning. We remark that in contrast to Shi et al. (2022); Wu et al. (2023); Song et al.

(2021), we *do not* assume the capability to sample from or evaluate $\pi(y | x)$. This section describes how we sample from $\pi(x | y)$ given a diffusion sampler for $\pi(x, y)$ without any additional training.

2.1 An abstract Gibbs sampler for the conditional distribution

Let us define a forward “noising” diffusion model

$$dY_t = \mu^Y(X_t, Y_t, t) dt + \sigma_t^Y dW_t^Y, \quad dX_t = \mu^X(X_t, Y_t, t) dt + \sigma_t^X dW_t^X, \quad (4)$$

with $(X_0, Y_0) \sim \pi$ and such that the pair (X_T, Y_T) is distributed according to *any* reference measure $\pi_T = \pi_{\text{ref}}$. We denote the measure associated with the diffusion (4) by \mathbb{F} . This type of SDE is typically given by standard diffusion models (Song et al., 2021) or Schrödinger bridges (De Bortoli et al., 2021, see also Appendix A).

The forward diffusion model can be associated with a denoising reverse-time diffusion model

$$dV_t = \mu^V(U_t, V_t, t) dt + \sigma_t^V dW_t^V, \quad dU_t = \mu^U(U_t, V_t, t) dt + \sigma_t^U dW_t^U, \quad (5)$$

such that if $(U_0, V_0) \sim \pi_{\text{ref}}$ then $(U_T, V_T) \sim \pi$ is distributed according to the target measure $\pi(x, y)$. We denote the measure associated with the backward diffusion (5) by \mathbb{B} . Our conditional sampler construction is based on the following abstract Gibbs sampler (Geman and Geman, 1984), which corresponds to alternatively propagating (4) from $t = 0$ to $t = T$, and then sampling U_T conditionally on $U_0 = X_T, V_0 = Y_T$, and $V_T = y$, coming from the forwards simulation pass. Formally, suppose that, at a Gibbs step $j \geq 0$, the path sample X_0^j is distributed according to $\pi(x | y)$ for a given y , and consider the following procedure:

1. sample $(Y_{(0,T]}^{j+1}, X_T^{j+1}) \sim \mathbb{F}(\cdot | X_0^j, Y_0 = y)$;
2. sample $X_0^{j+1} = U_T^{j+1} \sim \mathbb{B}(\cdot | U_0 = X_T^{j+1}, V_{[0,T]} = Y_{[T,0]}^{j+1})$.

Then, X_0^{j+1} is distributed according to the target $\pi(x | y)$.

In general, it is hard to directly apply the steps 1 and 2 above. Indeed, (i) at evaluation time, diffusion models are given in a discretised form, not in their continuous-time formulation, and (ii), even in their discretised form, the distributions arising in Steps 1 and 2 are not available in closed form. Next, we describe a practical MCMC algorithm targeting the discretised version of the two steps.

2.2 Discrete-time formulation

In Section 2.1, we have described an abstract procedure for sampling from the conditional model $\pi(\cdot | y)$ by iterative sampling from a conditioned forward noising process (step 1) and then running a conditioned version of the denoising SDE (step 2).

For this procedure to be practically implementable, we now assume that we have access to the discretised forward and backward SDEs, which are given marginally by

$$\begin{aligned} Y_{t_{k+1}} &\sim \mathbb{F}_{t_k}^Y(\cdot | Y_{t_k}, X_{t_k}), & V_{t'_{k+1}} &\sim \mathbb{B}_{t'_k}^V(\cdot | V_{t'_k}, U_{t'_k}), \\ X_{t_{k+1}} &\sim \mathbb{F}_{t_k}^X(\cdot | Y_{t_k}, X_{t_k}), & U_{t'_{k+1}} &\sim \mathbb{B}_{t'_k}^U(\cdot | V_{t'_k}, U_{t'_k}), \end{aligned} \quad (6)$$

where $t'_k = T - t_k, k = 0, \dots, K$, and form the diffusion model at hand².

Writing hereafter X_k and Y_k for X_{t_k} and Y_{t_k} (and similarly for U, V, \mathbb{F} , and \mathbb{B}), as well as the shorthands $X_{0:K} = (X_k)_{k=0}^K$ and $X_{K:0} = (X_k)_{k=K}^0$ for K time steps, the procedure described in Section 2.1 then becomes:

1. sample $(Y_{1:K}^{j+1}, X_K^{j+1}) \sim \mathbb{F}(\cdot | x_0 = X_0^j, y_0 = y)$;
2. sample $X_0^{j+1} = U_{K:0}^{j+1} \sim \mathbb{B}(\cdot | v_{0:K} = Y_{K:0}^{j+1}, u_0 = X_K^{j+1})$.

This structure of the conditional sampler was first introduced in Trippe et al. (2023, albeit not explicitly as a Gibbs sampler) for the special case when the drift in (1) is separable, namely when the

²For simplicity, we use the same notation for the continuous-time SDE and its (approximate) discretisation.

drifts μ^X and μ^Y in (1) do not depend on both Y and X , respectively (we come back to this special case in Section 3).

The simulation in step 1 is directly implementable. On the other hand, step 2 a well-studied problem in the literature on Bayesian filtering (see, e.g., Särkkä and Svensson, 2023), and approximate solutions are available, for example, in the form of particle filters (for a recent review of these see Chopin and Papaspiliopoulos, 2020) which were employed in Trippe et al. (2023). However, for a finite number of Monte Carlo samples used, these methods provide biased (despite consistency) samples from the filtering distribution, therefore resulting in a biased sampler for targeting $\pi(\cdot | y)$ in Trippe et al. (2023). Instead, we implement a Markov kernel \mathcal{K} keeping the filtering posterior $\mathbb{B}(u_{1:K} | v_{0:K}, u_0)$, for given $v_{0:K}$ and u_0 , invariant within the Gibbs sampler, resulting in the following structure:

1. sample $(Y_{1:K}^{j+1}, U_{K:0}^{j+1/2}) \sim \mathbb{F}(\cdot | x_0 = X_0^j, y_0 = y)$;
2. sample $X_{K:0}^{j+1} = U_{0:K}^{j+1} \sim \mathcal{K}(\cdot | X_{0:K}^{j+1/2})$, targeting $\mathbb{B}(u_{0:K} | v_{0:K} = Y_{K:0}^{j+1}, u_0 = X_T^{j+1/2})$.

The intermediary steps, including $X_{1:K}^{j+1}$ can then be discarded.

A natural algorithm for this purpose is given by *conditional sequential Monte Carlo* (CSMC, Andrieu et al., 2010), which modifies the standard particle filter algorithm into a Markov kernel. CSMC is known to be fast converging under weak conditions and scales well to long time horizons (Andrieu et al., 2018) as well as diminishing discretisation steps in continuous systems (provided an adequate implementation is used, see, e.g., Karppinen et al., 2023), including for as little as $N > 2$ Monte Carlo samples (Lee et al., 2020). We assume that the conditional transition density b_k^V of \mathbb{B}_k can be evaluated, and we provide pseudo-code for the CSMC algorithm (as well as the unconditional version, which we use later in Section 3) applied to step 2 above in Algorithm 1. For more details on both the unconditional and conditional versions of the algorithm, we refer to Chopin and Papaspiliopoulos (2020, Chap. 10 and 15, respectively) and Andrieu et al. (2010). In practice, to increase statistical efficiency, we use lower-variance resampling schemes and a final index selection step as in Karppinen et al. (2023); Chopin and Singh (2015).

Algorithm 1 Conditional/unconditional particle filter for $\mathcal{K}(\cdot | x_{0:K}^j)$.

input The current Markov chain state $x_{0:K}^j$, measurement path $y_{0:K}^j$, number of particles $N > 1$, and conditional flag $F \in \{0, 1\}$.

output An updated state x_0^{j+1} , and a marginal likelihood estimator Z^j .

- 1: Sample $U_1^n \sim \mathbb{B}_0(\cdot | y_K^j, x_K^j)$ for $n \in \{1, \dots, N\}$, and set $Z^j = 0$
 - 2: **if** $F = 1$ **then**
 - 3: Sample $n_0^* \sim \mathcal{U}[1, N]$, and set $U_0^{n_0^*} = x_K^j$.
 - 4: **end if**
 - 5: Set $w_1^n = b_1^V(y_{K-2}^j | y_{K-1}^j, U_1^n)$ for $n \in \{1, \dots, N\}$ and set $\ell_1 = \sum_{n=1}^N w_1^n$
 - 6: Normalise $w_1^n = w_1^n / \ell_1$ for $n \in \{1, \dots, N\}$, and $Z^j = \frac{1}{N} \times Z \times \ell_1$
 - 7: **for** $k = 2, \dots, K$ **do**
 - 8: Sample $A_k^n = i$ with probability w_{k-1}^i for $n \in \{1, \dots, N\}$
 - 9: Sample $U_k^n \sim \mathbb{B}_k(\cdot | y_{K-k}^j, U_{k-1}^{A_k^n})$ for $n \in \{1, \dots, N\}$
 - 10: **if** $F = 1$ **then**
 - 11: Sample $n_k^* \sim \mathcal{U}[1, N]$, and set $U_k^{n_k^*} = y_k^j$ and $A_k^{n_k^*} = n_{k-1}^*$
 - 12: **end if**
 - 13: Set $w_k^n = b_k^V(y_{K-k-1}^j | y_{K-k}^j, U_k^n)$ for $n \in \{1, \dots, N\}$ and set $\ell_k = \sum_{n=1}^N w_k^n$
 - 14: Normalise $w_k^n = w_k^n / \ell_k$ for $n \in \{1, \dots, N\}$, and $Z^j = \frac{1}{N} \times Z \times \ell_k$
 - 15: **end for**
 - 16: Sample $U_K^n \sim \mathbb{B}_{K-1}(\cdot | y_{K-1}^j, U_{K-1}^{A_K^n})$ for $n \in \{1, \dots, N\}$
 - 17: **if** $F = 1$ **then**
 - 18: Sample $n_K^* \sim \mathcal{U}[1, N]$, and set $U_K^{n_K^*} = x_0^j$ and $A_K^{n_K^*} = n_{K-1}^*$
 - 19: **end if**
 - 20: Sample $B_K \in \{1, \dots, N\}$ with probabilities $\{w_{K-1}^n\}_{n=1}^N$ and set $x_0^{j+1} = U_K^{B_K}$
-

Remark 2.1. When we are willing to make the assumption that $\pi_T \equiv \pi_{\text{ref}}$, then an alternative is to initialise Algorithm 1 with $U_0^n \sim \pi_{\text{ref}}$ rather than starting at $k = 1$ from $\mathbb{B}_0(\cdot \mid y_K^j, x_K^j)$.

3 Separable dynamics

The approach described in the previous section is generic, and in particular, it is applicable to non-separable noising SDEs, that is, those that have drifts μ^X and μ^Y that both depend on X and Y , such as the SDEs resulting from Schrödinger bridges. However, many diffusion models are derived from a separable forward noising SDE, typically given as an Ornstein–Uhlenbeck process, where μ^X only depends on X and μ^Y on Y . These models take the form

$$d \begin{bmatrix} Y_t \\ X_t \end{bmatrix} = A_t \begin{bmatrix} Y_t \\ X_t \end{bmatrix} dt + \Sigma_t dW_t \quad (7)$$

with block diagonal Σ_t and A_t . In this section, we describe how our approach can be further improved or adapted for these models.

3.1 Improving the efficiency of the CSMC

In the case when the forward-noising dynamics are given by an SDE of the form (7), the conditional trajectories $\mathbb{F}(\cdot \mid x_T, y_T, x_0, y_0)$ are tractable, which allows improving the procedure outlined in Section 2 by implementing step 1 as simulating a diffusion bridge. Namely, instead of simulating the dynamics $\mathbb{F}(\cdot \mid X_0^j, y)$ forward and storing the result to then feed the CSMC sampler, we can obtain X_T^j, Y_T^j either from the forward simulation (or from π_{ref} if it is trusted) and then implement the bridge backwards in time, simulating $\mathbb{F}(x_k, y_k \mid x_{k+1}^j, y_{k+1}^j, x_0, y_0)$ online rather than storing the full path. This is particularly useful for high-dimensional distributions for which samples are expensive to store.

Remark 3.1. We note that this can be done approximately in the context of non-separable nonlinear SDEs (Bladt et al., 2016), for example, arising from Schrödinger bridges. However, since we specifically focus on exact conditioning, we elect not to treat this case here.

3.2 A pseudo-marginal implementation

When the forward noising process is given as in (7), we can implement a pseudo-marginal counterpart of Section 2, known as the particle Markov chain Monte Carlo (PMCMC) method, or more precisely the particle marginal Metropolis–Hastings (PMMH) algorithm (Andrieu et al., 2010). This approach relies on the fact that particle filtering returns an unbiased estimate of the marginal likelihood of the path $Y_{1:K}$ under \mathbb{B} , given as $\prod_{k=1}^K \frac{1}{N} \sum_{n=1}^N w_k^n$, outputted by Algorithm 1 (with $F = 0$), which can be used in a Metropolis–Hastings step to sample from the posterior distribution of the path $X_{0:K}$. In the context of our problem, this corresponds to the following procedure. Given X_0^j distributed according to $\pi(\cdot \mid y)$ and an unbiased estimator of the marginal likelihood Z^j of $\mathbb{B}(y_{K:0}) = \int \mathbb{B}(y_{K:0}, du_{0:K})$:

1. propose a path $Y_{1:K}^*$ from a proposal distribution $q(\cdot \mid Y_{0:K}^j)$ keeping $\mathbb{F}(dy_{1:K} \mid y_0 = y)$ invariant^a;
2. run Algorithm 1 (with $F = 0$) targeting $\mathbb{B}(\cdot \mid Y_{K:0}^*)$ to obtain a marginal likelihood estimate Z^* and a proposed X_0^* ;
3. set $\alpha = \frac{Z^*}{Z^j}$;
4. set $X_0^{j+1} = X_0^*$, $Z^{j+1} = Z^*$, and $Y_{1:K}^{j+1} = Y_{1:K}^*$ with probability $1 \wedge \alpha$, otherwise set $X_0^{j+1} = X_0^j$, $Z^{j+1} = Z^j$, and $Y_{1:K}^{j+1} = Y_{1:K}^j$.

^aIt is possible to use other proposals, not reversible with respect to $\mathbb{F}(\cdot \mid y_0)$, but this would require modifying the acceptance probability in step 3 to account for the difference introduced by the proposal.

The algorithm above marginally keeps $\pi(\cdot \mid y)$ invariant under the sole assumption that $\pi_T = \pi_{\text{ref}}$.

Remark 3.2. In step 1, we take an $\mathbb{F}(\cdot \mid y_0)$ -invariant kernel. In this work, we choose the preconditioned Crank–Nicolson (PCN, Cotter et al., 2013) proposal, which is well adapted to Gaussian priors

Table 1: Errors statistics for the the conditional sampling problem of Section 4.1. The left and right panels show the errors when using 10 and 100 particles, respectively. The columns “Mean” and “Variance” report the errors in the marginal mean and variance of the posterior distribution. The number after PMCMC is the PCN parameter δ applied. Note that the CSGM approach can be computed exactly, we therefore use it as the reference and do not compete against it here.

	KL	Bures	Mean ($\times 10^{-2}$)	Variance ($\times 10^{-2}$)	KL	Bures	Mean ($\times 10^{-2}$)	Variance ($\times 10^{-2}$)
PF	1.67 \pm 0.12	0.71 \pm 0.10	4.51 \pm 0.74	4.02 \pm 0.05	1.12 \pm 0.07	0.29 \pm 0.05	3.12 \pm 0.49	2.33 \pm 0.05
Gibbs-CSMC	1.05 \pm 0.01	0.07 \pm 0.00	0.88 \pm 0.08	0.41 \pm 0.03	0.76 \pm 0.00	0.04 \pm 0.00	0.54 \pm 0.04	0.32 \pm 0.02
PMCMC-0.005	26.31 \pm 1.41	1.22 \pm 0.09	4.45 \pm 0.45	1.74 \pm 0.12	22.11 \pm 1.04	1.18 \pm 0.08	5.01 \pm 0.47	1.73 \pm 0.11
PMCMC-0.001	6.83 \pm 0.57	0.50 \pm 0.07	3.48 \pm 0.39	1.24 \pm 0.08	4.50 \pm 0.21	0.55 \pm 0.07	4.68 \pm 0.45	1.50 \pm 0.07
TPF	5.22 \pm 0.67	1.32 \pm 0.56	6.04 \pm 1.92	2.26 \pm 0.47	2.61 \pm 0.34	0.78 \pm 0.32	5.84 \pm 0.02	1.09 \pm 0.50
CSGM-exact	0.66 \pm 0.01	0.03 \pm 0.00	0.33 \pm 0.04	0.20 \pm 0.02	←	←	←	←

such as (7). Noting that $\mathbb{F}(y_{1:K} | y_0 = y)$ is a linear transformation of Gaussian variables η , and writing η^j for those corresponding to $Y_{1:K}^j$, this consists in sampling q as follows: given a step size $\delta > 0$, (i) sample $\eta' \sim \mathcal{N}(0, I)$, (ii) set $\eta^* = \frac{2}{2+\delta} \eta^j + \sqrt{1 - \frac{4}{4+4\delta+\delta^2}} \eta'$, and (iii) form Y^* from η^* . Importantly, this can be done with zero memory cost if one has access to the random number generator that was used to sample η^j originally, in which case we can simply re-simulate η^j alongside η' at zero memory cost and negligible (compared to evaluating the SDE drift) computational cost.

4 Experiments

In this section, we conduct quantitative and qualitative experiments to validate our proposed method (i.e., Gibbs-CSMC in Sections 2.1 and 3.1 and PMCMC in Section 3.2) on both synthetic and real data. We compare to the methods most related to ours: the standard particle filter (PF, Trippe et al., 2023; Dou and Song, 2024), twisted particle filter (TPF, Wu et al., 2023), and conditional score matching (CSGM, Song et al., 2021). Throughout our experiments, when a particle filter is used, we implement it using stratified resampling (see, e.g., Chopin and Papaspiliopoulos, 2020, Chap. 9), and when we use a conditional particle filter, we implement it using the conditional “killing” resampling of Karppinen et al. (2023), rather than the multinomial resampling as described in Algorithm 1. Unless otherwise mentioned, we repeat every experiment 100 times independently, and we report the statistics (i.e., mean, standard deviation, and/or quantile) of their results. For ease of reproducibility, we publish our implementations at <https://github.com/zgbkdlm/fbs>.

4.1 High-dimensional synthetic conditional sampling

In our first experiment, we assess the convergence of all the conditioning methods considered to the ‘true’ conditional distribution. To do so, we set the target $\pi(x | y)$ as the posterior distribution of a Gaussian process (GP) regression model for which the ground truth is available. We choose a standard Ornstein–Uhlenbeck forward noising process, for which we can compute the reverse SDE (2) exactly, removing the discretisation bias to isolate the error coming from the conditioning only. For each method, we generate 10,000 posterior samples, and then compute how these samples approximate the true posterior distribution in terms of Kullback–Leibler (KL) divergence, Wasserstein–Bures (Bures) distance, and mean absolute errors of the marginal means and variances. The detailed experimental setting is given in Appendix B.2.

As demonstrated by Table 1, Gibbs-CSMC significantly outperforms all other methods for all metrics. Importantly, the Gibbs-CSMC method is substantially better than PF, showing that our MCMC strategy effectively corrects the bias of the PF approach of Trippe et al. (2023). Our PMCMC approach also improves upon PF but is sensitive to the calibration of the PCN parameter δ . Specifically, when $\delta = 0.005$, the KL of PMCMC is the worst, and decreasing it to $\delta = 0.001$ improves the errors. On the other hand, the marginal mean and variance errors of PMCMC are relatively good, compared to KL, indicating that the method does not approximate well the off-diagonal part of the GP posterior covariance. The results of TPF appear to be worse than PF, and also have larger standard deviations. Finally, we also see from the table that increasing the number of particles improves the errors for all methods. More qualitative results are given in Appendix B.2.

Figure 1 plots the autocorrelations of our Gibbs-CSMC and PMCMC methods. We see that the autocorrelation of Gibbs-CSMC is better than PMCMC, even when using a lower number of particles. We also observe that the autocorrelation of PMCMC can be improved by decreasing the PCN

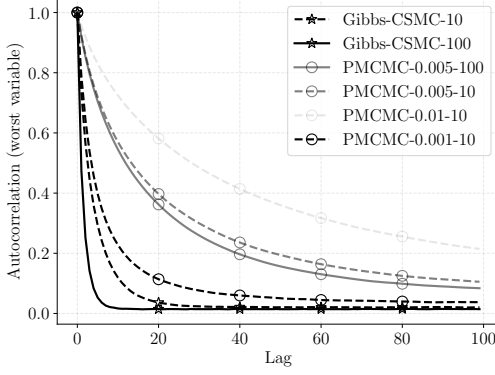


Figure 1: Autocorrelations of PMCMC and Gibbs-CSMC in Section 4.1. For each of the 100 dimensions we compute the autocorrelation averaged over four independent chains. We then report the autocorrelation of the worst dimension. We see that Gibbs-CSMC is better than PMCMC, and that increasing the number of particles improves the autocorrelation.

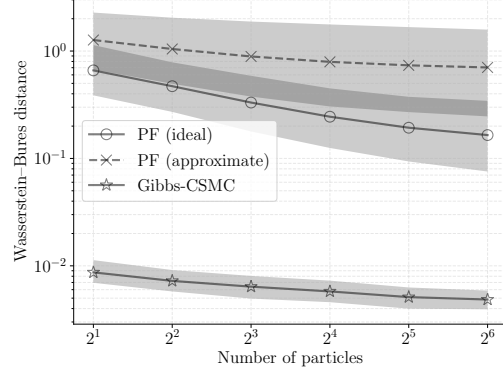


Figure 2: Conditional sampling errors on a Gaussian Schrödinger bridge. PF (ideal) refers to using the exact posterior distribution (which is not available in general) to initialise PF, whereas PF (approximate) uses a standard Normal at initialisation. Gibbs sampling improves the sampling quality *even compared to PF (ideal)*, highlighting the incorrectness of PF.

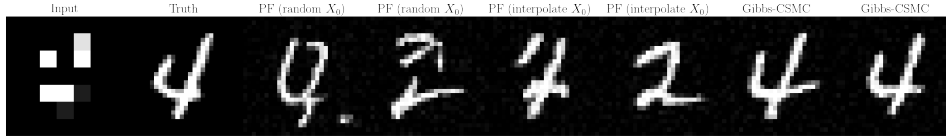


Figure 3: MNIST super-resolution ($\times 4$) on a (non-separable) Schrödinger bridge noisy process. For each method, we show two samples (more samples are shown in Figure 7). We find that PF is significantly affected by its initialisation of X_0 , while our Gibbs-CSMC method barely suffers from this problem.

parameter δ . This is mostly due to the variance of the log-likelihood estimation (see Section 3.2) of the PMCMC method (Andrieu and Roberts, 2009; Doucet et al., 2015), sometimes preventing the algorithm from moving, and which is negatively affected by δ . Lastly, the figure also confirms that increasing the number of particles improves the autocorrelations overall.

4.2 Conditional sampling on non-separable noisy processes

One key merit of our method is its generalisability: it works on non-separable noisy processes as well as separable ones. Precisely, our method does not need X_t and Y_t of the noising process in (4) to be independent conditionally on X_0 and Y_0 . On the other hand, the separability is a requirement for the standard PF approach of Dou and Song (2024); Trippe et al. (2023). Indeed, when the noising process is non-separable, their approach requires us to sample X_0 in order to generate a path $t \mapsto Y_t$. Ideally, $X_0 \sim \pi(x | y)$ should come from the true conditional distribution, but in reality, we have to use approximate conditional samplers, which incur additional biases that are hard to eliminate.

To quantify the bias arising from the non-separability, we perform conditional sampling on a Gaussian Schrödinger bridge model (for which closed-form expressions are available, see, e.g., Bunne et al., 2023) using our Gibbs-CSMC approach and the PF of Trippe et al. (2023). We do not compare to our PMCMC approach given its non-applicability here (see Section 3.2). We continue working on the same GP regression problem in Section 4.1, but, to highlight further the impact of non-separability, rather than using a reference $\mathcal{N}(0, I)$, we use $\pi_T \sim \mathcal{N}(0, \Sigma)$, where Σ is a random covariance matrix drawn from a Wishart distribution. The results are shown in Figure 2. We see that approximating the initial $\pi(x | y)$ introduces significant errors compared to the PF using exact initial sampling. Moreover, increasing the number of particles does not compensate for this initial bias highlighting the defect of the standard approach in non-separable models.

Table 2: Results of MNIST inpainting and super-resolution. In the left and right panels, we show the results using 10 and 100 particles, respectively. Bold numbers are the best column-wise.

MNIST	Inpainting		Super-resolution		Inpainting		Super-resolution	
	PSNR	SSIM	PSNR	SSIM	PSNR	SSIM	PSNR	SSIM
PF	15.85	0.74	10.14	0.32	17.34	0.79	11.66	0.45
Gibbs-CSMC	16.79	0.77	10.84	0.38	17.82	0.82	14.06	0.61
PMCMC-0.005	17.51	0.80	12.88	0.54	17.84	0.81	14.22	0.63
TPF	13.45	0.48	9.67	0.19	13.89	0.51	10.38	0.25
CSGM	15.17	0.71	9.72	0.28	←	←	←	←

Table 3: Results of CelebA-HQ inpainting and super-resolution. In the left and right panels, we apply 2 and 10 particles, respectively. Bold numbers are the best column-wise.

CelebA-HQ	Inpainting			Super-resolution			Inpainting			Super-resolution		
	PSNR	SSIM	LPIPS	PSNR	SSIM	LPIPS	PSNR	SSIM	LPIPS	PSNR	SSIM	LPIPS
PF	22.88	0.85	0.05	23.29	0.79	0.11	23.98	0.87	0.04	24.57	0.82	0.09
Gibbs-CSMC	22.86	0.86	0.05	23.75	0.80	0.11	24.22	0.87	0.04	25.07	0.84	0.09
PMCMC-0.005	23.96	0.87	0.04	24.37	0.82	0.10	24.68	0.88	0.04	25.30	0.85	0.07
TPF	13.79	0.59	0.20	12.71	0.44	0.23	13.93	0.58	0.20	12.92	0.45	0.23
CSGM	22.86	0.85	0.05	23.48	0.79	0.11	←	←	←	←	←	←

We also qualitatively show the results for MNIST super-resolution on a pre-trained Schrödinger bridge. This time, we no longer have access to an exact X_0 sampler for the PF method, and we here use a uniform random X_0 , and an X_0 using linear interpolation of y_0 . The results are shown in Figure 3. We see from this figure that the initial specification of X_0 appearing in the forward noising process significantly impacts the results. When using a random X_0 , where all pixels are uniform $\mathcal{U}(0, 1)$, the recovered images deviate significantly from the truth. When using linear interpolation, which is a better initialisation, the recovered images look closer to the truth, but the quality is still poor. On the other hand, Gibbs-CSMC does not suffer from this initialisation problem and recovers the original digit as the MCMC chain converges. More results are given in Appendix B.3.

4.3 Inpainting and super-resolution

In this section, we apply our methods for inpainting and super-resolution on MNIST (resolution 28 by 28) and CelebA-HQ (resolution 64 by 64) images. For a complete description of the inpainting and super-resolution problems and additional experimental details, we refer the reader to Appendix B.4.

Given pre-trained (via the standard score matching method of Song et al., 2021) unconditional generative diffusions for MNIST and CelebA-HQ images, we then perform conditional sampling of missing (inpainting) or deblurred (super-resolution) of images given an observation thereof. To quantify the results, for each test image we recover 100 conditional image samples, and we compute the peak signal-to-noise ratio (PSNR), structural similarity index (SSIM), and learnt perceptual patch similarity (LPIPS, Zhang et al., 2018) metrics averaged over the 100 samples.

The results are summarised in Tables 2 and 3. We see that our PMCMC approach is the best in terms of all the metrics, followed by Gibbs-CSMC. Importantly, our PMCMC and Gibbs-CSMC methods outperform the PF approach, showing that our MCMC framework indeed compensates the bias exhibited by PF for real applications. The classical CSGM approach performs similarly as PF, however, the filtering-based approaches can be systematically improved by increasing the number of particles, while CSGM cannot.

In Figure 4, we illustrate the methods for inpainting and super-resolution on a single task. We see that PF, TPF, and CSGM can generate unrealistic samples, and the super-resolution samples are sometimes contaminated by pixel distortions (e.g., the isolated white dots in the second panel, first row, third-fifth columns in the figure). This is particularly true for TPF despite it largely higher computational cost (due to taking gradient with respect to the score function in its twisting function, Wu et al., 2023) as it requires to further approximate the likelihood model $\pi(y | x)$ by a smoother version to be usable.

However, our Gibbs-CSMC and PMCMC methods tend to produce better quality samples, albeit more correlated ones, as those wrong samples are rejected by the MCMC kernel. For more examples and results, we refer the readers to Appendix B.4.

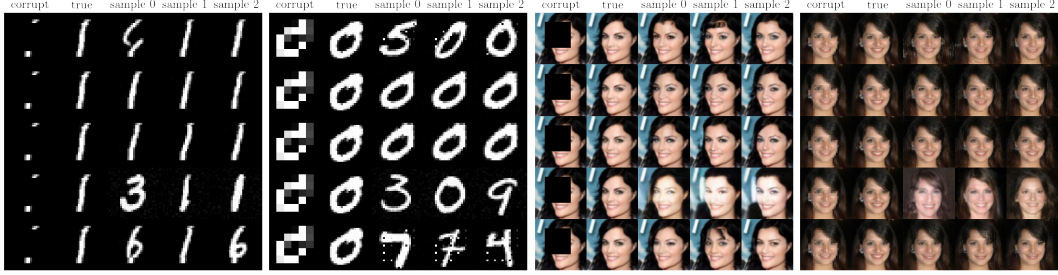


Figure 4: Examples of inpainting (first and third panels) and super-resolution (second and fourth panels) on MNIST and CelebA-HQ. In each panel, the first to the last rows show the results of PF, Gibbs-CSMC, PMCMC-0.005, TPF, and CSGM, respectively. We see that the samples generated by Gibbs-CSMC and PMCMC have overall better quality.

5 Related works

In the past few years, several methods have been proposed to perform conditional sampling within diffusion models. The first way to do so was proposed alongside score-based denoising diffusion models in the landmark work by Song et al. (2021). They rely on learning an approximate conditioning drift model *after* the fact, adding a layer of approximate learning on top of the unconditional one. This type of idea can also be found in Shi et al. (2022) who train a Schrödinger bridge on the joint distribution of the latent variable X and the observed Y when the model $\pi(y | x)$ is available. Closer to our work, Wu et al. (2023) propose using a twisted particle filter (Whiteley and Lee, 2014) to efficiently bridge between the reference distribution and the conditional $\pi(x | y)$ at the cost of additional expensive computations in the procedure. Finally, Trippe et al. (2023), as well as the contemporaneous Dou and Song (2024), express the problem of conditioning as a bridge for simulated observations too. In fact, Trippe et al. (2023) is exactly given as a special case of Section 3.2 where the new path is proposed independently from the previous one (i.e., in our formulation, $q \equiv \mathbb{F}(\cdot | y_0)$), and the resulting sample is accepted unconditionally (i.e., their method is equivalent to setting $\alpha = 1$), ignoring the fact that two Y paths sampled under the forward dynamics (the prior) may have different marginal likelihoods under the backward denoising model. This means that their method is inherently biased and does not asymptotically target the right distribution, despite their consistency result, even under the assumption $\pi_T \equiv \pi_{\text{ref}}$. The resulting bias is reflected in our experiments. This defect is shared by Dou and Song (2024). Additional background details can be found in Appendix A.

6 Conclusion

We have presented a novel MCMC-based method for sampling from conditional distributions expressed as diffusion models and Schrödinger bridges. Our method relies on formulating the sampling procedure as an inference problem on missing observation data, thanks to which we can apply classical particle MCMC algorithms (Andrieu et al., 2010) to perform (asymptotically) exact sampling within the model. We have demonstrated the performance and correctness of our method on simulated and real datasets, for inpainting and super-resolution problems alike.

While our method improves on the pre-existing methodology, in particular Trippe et al. (2023) on which we generalise, several questions remain open. In particular, (i) while we did not directly report on this, we observed that the distribution of the particles in the backward filtering pass contracts at the terminal time (Trippe et al., 2023; Wu et al., 2023, this is true for all methods considered here, including), and may consequently increase the autocorrelation of our MCMC chains, explaining their lack of diversity despite the overall improvement in quality. Because this appears throughout, it seems to be a feature of the model decomposition rather than a feature of Gibbs-CSMC or PMCMC. (ii) We also notice that the variance of the log-likelihood estimation in PMCMC can be large, and hence, its acceptance rate can be unstable, also making the calibration of its step-size difficult. While this is detrimental to our approach, it also explains the poor posterior coverage of Trippe et al. (2023) who completely ignore this step.

Consequently, to obtain independent samples with adequate posterior coverage, a pragmatic compromise is likely to repeatedly use Trippe et al. (2023) as initialisation and then correct the posterior

sample by running our methods for a few iterations. Nevertheless, solving both these issues is of great interest, and is likely feasible within the framework we outlined in this article by a more careful consideration of the structure of the augmented model. We leave these questions for future work.

Individual Contributions

The original idea and methodology are due to AC and subsequently refined jointly by AC and ZZ. Implementation and experimental evaluation are mostly due to ZZ with help and inputs from AC. Writing was primarily done by AC with substantial help from ZZ and inputs from TS. All authors edited and validated the final manuscript.

Acknowledgement

This work was partially supported by the Kjell och Märta Beijer Foundation, and Wallenberg AI, Autonomous Systems and Software Program (WASP) funded by the Knut and Alice Wallenberg Foundation. The computations were enabled by the Berzelius resource provided by the Knut and Alice Wallenberg Foundation at the National Supercomputer Centre. Adrien Corenflos and Simo Särkkä were partially supported by the Research Council of Finland. Adrien Corenflos also acknowledges the financial support provided by UKRI for OCEAN (a 2023-2029 ERC Synergy grant co-sponsored by UKRI).

References

- Christophe Andrieu and Gareth O. Roberts. The pseudo-marginal approach for efficient Monte Carlo computations. *The Annals of Statistics*, 37(2):697–725, 2009.
- Christophe Andrieu, Arnaud Doucet, and Roman Holenstein. Particle Markov chain Monte Carlo methods. *Journal of the Royal Statistical Society: Series B (Statistical Methodology)*, 72(3): 269–342, 2010. With discussion.
- Christophe Andrieu, Anthony Lee, and Matti Vihola. Uniform ergodicity of the iterated conditional SMC and geometric ergodicity of particle Gibbs samplers. *Bernoulli*, 24(2):842–872, 2018.
- Mogens Bladt, Samuel Finch, and Michael Sørensen. Simulation of multivariate diffusion bridges. *Journal of the Royal Statistical Society Series B: Statistical Methodology*, 78(2):343–369, 2016.
- James Bradbury, Roy Frostig, Peter Hawkins, Matthew James Johnson, Chris Leary, Dougal Maclaurin, George Necula, Adam Paszke, Jake VanderPlas, Skye Wanderman-Milne, and Qiao Zhang. JAX: composable transformations of Python+NumPy programs, 2018. URL <http://github.com/google/jax>.
- Charlotte Bunne, Ya-Ping Hsieh, Marco Cuturi, and Andreas Krause. The Schrödinger bridge between Gaussian measures has a closed form. In *Proceedings of The 26th International Conference on Artificial Intelligence and Statistics*, volume 206, pages 5802–5833. PMLR, 25–27 Apr 2023.
- Gabriel Cardoso, Yazid Janati el idrissi, Sylvain Le Corff, and Eric Moulines. Monte Carlo guided denoising diffusion models for Bayesian linear inverse problems. In *The 12th International Conference on Learning Representations*, 2024.
- Yongxin Chen, Tryphon T. Georgiou, and Michele Pavon. Optimal transport in systems and control. *Annual Review of Control, Robotics, and Autonomous Systems*, 4:89–113, 2021.
- Nicolas Chopin and Omiros Papaspiliopoulos. *An Introduction to Sequential Monte Carlo*. Springer, 2020.
- Nicolas Chopin and Sumeetpal S. Singh. On particle Gibbs sampling. *arXiv preprint arXiv:1304.1887 version 1*, 2015.
- S. L. Cotter, G. O. Roberts, A. M. Stuart, and D. White. MCMC methods for functions: modifying old algorithms to make them faster. *Statistical Science*, 28(3):424–446, 2013.
- Valentin De Bortoli, James Thornton, Jeremy Heng, and Arnaud Doucet. Diffusion Schrödinger bridge with applications to score-based generative modeling. In *Advances in Neural Information Processing Systems*, volume 34, pages 17695–17709, 2021.
- Zehao Dou and Yang Song. Diffusion posterior sampling for linear inverse problem solving: a filtering perspective. In *Proceedings of the Twelfth International Conference on Learning Representations*, 2024.
- Arnaud Doucet, Michael K Pitt, George Deligiannidis, and Robert Kohn. Efficient implementation of Markov chain Monte Carlo when using an unbiased likelihood estimator. *Biometrika*, 102(2): 295–313, 2015.
- Stuart Geman and Donald Geman. Stochastic relaxation, Gibbs distributions, and the Bayesian restoration of images. *IEEE Transactions on Pattern Analysis and Machine Intelligence*, 6(6): 721–741, 1984.
- Jonathan Heek, Anselm Levskaya, Avital Oliver, Marvin Ritter, Bertrand Rondepierre, Andreas Steiner, and Marc van Zee. Flax: A neural network library and ecosystem for JAX, 2023. URL <http://github.com/google/flax>.
- Jonathan Ho, Ajay Jain, and Pieter Abbeel. Denoising diffusion probabilistic models. In *Advances in Neural Information Processing Systems*, volume 33, pages 6840–6851, 2020.
- Aapo Hyvärinen. Estimation of non-normalized statistical models by score matching. *Journal of Machine Learning Research*, 6(24):695–709, 2005.
- Ioannis Karatzas and Steven E. Shreve. *Brownian Motion and Stochastic Calculus*, volume 113 of *Graduate Texts in Mathematics*. Springer-Verlag New York, 2nd edition, 1991.
- Santeri Karppinen, Sumeetpal S. Singh, and Matti Vihola. Conditional particle filters with bridge backward sampling. *Journal of Computational and Graphical Statistics*, 0(0):1–15, 2023.

- Diederik Kingma and Jimmy Ba. Adam: A method for stochastic optimization. In *International Conference on Learning Representations (ICLR)*, 2015.
- Anthony Lee, Sumeetpal S Singh, and Matti Vihola. Coupled conditional backward sampling particle filter. *Annals of Statistics*, 48(5):3066–3089, 2020.
- Christian Léonard. A survey of the Schrödinger problem and some of its connections with optimal transport. *Discrete and Continuous Dynamical Systems*, 34(4):1533–1574, 2014.
- Ziwei Liu, Ping Luo, Xiaogang Wang, and Xiaoou Tang. Deep learning face attributes in the wild. In *Proceedings of International Conference on Computer Vision (ICCV)*, pages 3730–3738, 2015.
- Ilya Loshchilov and Frank Hutter. SGDR: Stochastic gradient descent with warm restarts. In *International Conference on Learning Representations*, 2017.
- Ziwei Luo, Fredrik K. Gustafsson, Zheng Zhao, Jens Sjölund, and Thomas B. Schön. Image restoration with mean-reverting stochastic differential equations. In *Proceedings of the 40th International Conference on Machine Learning*, volume 202, pages 23045–23066. PMLR, 2023.
- Gael M. Martin, David T. Frazier, and Christian P. Robert. Computing Bayes: from then ‘til now. *Statistical Science*, 39(1):1–17, 2023.
- Sean P. Meyn and Richard L. Tweedie. *Markov chains and stochastic stability*. Cambridge University Press, 2nd edition, 2009.
- Leonard Christopher Gordon Rogers and David Williams. *Diffusions, Markov Processes, and Martingales*. Cambridge University Press, 2nd edition, 2000.
- Simo Särkkä and Lennart Svensson. *Bayesian filtering and smoothing*, volume 17. Cambridge university press, 2023.
- Yuyang Shi, Valentin De Bortoli, George Deligiannidis, and Arnaud Doucet. Conditional simulation using diffusion Schrödinger bridges. In *Proceedings of the 38th Conference on Uncertainty in Artificial Intelligence*, volume 180, pages 1792–1802. PMLR, 2022.
- Yuyang Shi, Valentin De Bortoli, Andrew Campbell, and Arnaud Doucet. Diffusion Schrödinger bridge matching. In *Advances in Neural Information Processing Systems*, volume 36, 2023.
- Jiaming Song, Chenlin Meng, and Stefano Ermon. Denoising diffusion implicit models. In *International Conference on Learning Representations*, 2020.
- Yang Song and Stefano Ermon. Improved techniques for training score-based generative models. In *Advances in Neural Information Processing Systems*, volume 33, pages 12438–12448, 2020.
- Yang Song, Jascha Sohl-Dickstein, Diederik P. Kingma, Abhishek Kumar, Stefano Ermon, and Ben Poole. Score-based generative modeling through stochastic differential equations. In *Proceedings of the 9th International Conference on Learning Representations*, 2021.
- Brian L. Trippe, Jason Yim, Doug Tischer, David Baker, Tamara Broderick, Regina Barzilay, and Tommi S. Jaakkola. Diffusion probabilistic modeling of protein backbones in 3D for the motif-scaffolding problem. In *Proceedings of The 11th International Conference on Learning Representations*, 2023.
- G. E. Uhlenbeck and L. S. Ornstein. On the theory of the Brownian motion. *Physical Review*, 36(5): 823–841, 1930.
- Francisco Vargas, Will Grathwohl, and Arnaud Doucet. Denoising diffusion samplers. In *Proceedings of the 11th International Conference on Learning Representations*, 2023.
- Nick Whiteley and Anthony Lee. Twisted particle filters. *The Annals of Statistics*, 42(1):115 – 141, 2014.
- Luhuan Wu, Brian Trippe, Christian Naeseth, David Blei, and John P Cunningham. Practical and asymptotically exact conditional sampling in diffusion models. In *Advances in Neural Information Processing Systems*, volume 36, pages 31372–31403. Curran Associates, Inc., 2023.
- Richard Zhang, Phillip Isola, Alexei A. Efros, Eli Shechtman, and Oliver Wang. The unreasonable effectiveness of deep features as a perceptual metric. In *Proceedings of the IEEE Conference on Computer Vision and Pattern Recognition (CVPR)*, pages 586–595, June 2018.

A Additional background

In this section we present additional background on generative diffusions in general. In particular, we show the foundation of sampling within generative diffusions, and how we can further leverage generative diffusions for conditional sampling.

A.1 Unconditional generative models

There are two popular classes of diffusion-based generative models in the community, that are, denoising diffusion models, and Schrödinger bridges.

A.1.1 Denoising diffusion models

Denoising diffusion models (Song et al., 2021) have recently received a lot of attention as a general-purpose sampler for generative modelling (Song et al., 2021) or statistical inference (Vargas et al., 2023). At the core, given a target distribution π_0 and a time-homogeneous stochastic differential equation (SDE)

$$dX_t = f(X_t) dt + dW_t, \quad X_0 \sim \pi_0, \quad (8)$$

with stationary distribution π_{ref} , they sample from π_0 by “denoising” (8) by means of Doob’s h -transform (Rogers and Williams, 2000). Formally, let π_t be the distribution of X_t under (8), and assume that we know how to sample from π_T for some $T > 0$. We can obtain approximate samples from π_0 by sampling from

$$\begin{aligned} dU_t &= f_{\text{rev}}(U_t, t) dt + dB_t, \\ U_0 &\sim \pi_T, \end{aligned} \quad (9)$$

where B is another Brownian motion, and we write $f_{\text{rev}}(U_t, t) := -f(U_t) + \nabla \log \pi_{T-t}(U_t)$.

When $T \gg 1$, and under ergodicity guarantees (Meyn and Tweedie, 2009), $\pi_T \approx \pi_{\text{ref}}$, so that if (8) is chosen such that π_{ref} is easy to sample from, then the only remaining blocker is computing the score $\nabla \log \pi_{T-t}$. However, obtaining an expression for π_t (and therefore for $\nabla \log \pi_{T-t}$) is in general not possible, and denoising diffusion models usually rely on score matching (Hyvärinen, 2005), whereby an approximation $s_{\theta^*}(t, x_t)$ to $\nabla \log \pi_t$ is learnt under samples by minimising the loss function

$$\mathcal{L}(\theta) = \int_0^T \mathbb{E} \left[\|s_{\theta}(X_t, t) - \nabla \log \pi_t(X_t | X_0)\|^2 dt \right], \quad (10)$$

with the expectation being taken under \mathbb{P} in (8). In practice, the method is implemented in discrete time, SDEs are sampled using numerical integrators, and the loss (10) becomes

$$\begin{aligned} \mathcal{L}(\theta) &= \sum_{k=1}^K \mathbb{E} \left[\|s_{\theta}(X_{t_k}, t_k) - \nabla \log \pi_{t_k}(X_{t_k} | X_0)\|^2 \right] \\ &= \sum_{k=1}^K \mathbb{E} \left[\|s_{\theta}(X_{t_k}, t_k) - \nabla \log \pi_{t_k}(X_{t_k} | X_{t_{k-1}})\|^2 \right], \end{aligned} \quad (11)$$

with $0 = t_0 < t_1 < \dots < t_K = T$ being a given integration grid used also at evaluation time to simulate from (9). When (8) is chosen, as is often the case, to be linear (for example, as an Ornstein–Uhlenbeck process, Uhlenbeck and Ornstein, 1930), $\pi_t(\cdot | X_0)$ can be computed and sampled from exactly so that the first version of (11) incurs no error other than the sampling noise. When it is not, as in the next section, the second version is more amenable to computations (and is also more numerically stable), at the cost of storing trajectories under \mathbb{P} .

A.1.2 Schrödinger bridges

A strong drawback of denoising diffusion models lies in the assumption $T \gg 1$, under which X_T is only approximately distributed according to π_{ref} . Under this assumption, the denoising process (9) will need to be numerically simulated for a large number of steps K , resulting in an inefficient and expensive procedure for both training and testing procedures. To mitigate this, it is preferable to explicitly bridge between the distributions π_0 and π_{ref} in a finite-time horizon, that is, find a forward

SDE (8) and a time reversal (9) such that π_T is exactly π_{ref} for a finite T . There are infinitely many such bridges, and in practice, we resort to the one that is in some sense easy to simulate.

Schrödinger bridges (Léonard, 2014; Chen et al., 2021) constitute a class of bridges which aim at minimising the total energy expense to move from π_0 to π_T and vice versa. Given a reference path measure \mathbb{Q} on the set of continuous paths $\mathcal{C}([0, T], \mathbb{R}^d) =: \mathcal{C}$, the Schrödinger bridge solution \mathbb{P}^{SB} is defined as the (unique) solution to

$$\mathbb{P}^{\text{SB}} = \arg \min_{\mathbb{P} \in \mathcal{P}(\mathcal{C})} \{ \text{KL}(\mathbb{P} \parallel \mathbb{Q}) \mid \mathbb{P}_0 = \pi_0, \mathbb{P}_T = \pi_T \}, \quad (12)$$

where $\mathcal{P}(\mathcal{C})$ denotes all the path measures on \mathcal{C} . In general, solving (12) directly is not possible, and instead, one needs to rely on alternative ways of solving the Schrödinger bridge. The two main methods to do so are given by iterative proportional fitting (IPF, De Bortoli et al., 2021) and Schrödinger bridge matching (SBM, Shi et al., 2023) which we review below.

The IPF method follows from the fact that the solution of (12) is given by the fixed point of a sequence of time-reversal operations: starting from $\mathbb{P}^0 = \pi_0 \mathbb{Q}_{|0}$, one constructs a sequence $\mathbb{P}^{2n+1} = \pi_T \{ \iota \mathbb{P}^{2n} \}_{|T}$, $\mathbb{P}^{2n+2} = \pi_0 \{ \iota \mathbb{P}^{2n+1} \}_{|T}$ by iteratively learning the time-reversal $\iota \mathbb{P}^n$ of the previous bridge \mathbb{P}^n , where we denote ι as a time-reversal operation.

The SBM method is given by the characterisation of \mathbb{P}^{SB} as the unique measure in the set of Markov processes \mathcal{M} which also belongs to the reciprocal class of \mathbb{Q} , i.e., $\mathcal{R}(\mathbb{Q}) := \{ \mathbb{P} \in \mathcal{P}(\mathcal{C}) \mid \mathbb{P} = \mathbb{P}_{0,T} \mathbb{Q}_{|0,T} \}$ defined as the set of measures that correspond to bridges under the dynamics of \mathbb{Q} . To find the Schrödinger bridge \mathbb{P}^{SB} , one can then construct a sequence of measures in $\mathcal{P}(\mathcal{C})$ as follows: $\mathbb{P}^0 = (\pi_0 \otimes \pi_T) \mathbb{Q}_{|0,T} \in \mathcal{R}(\mathbb{Q})$, and then iteratively project the approximate measure onto \mathcal{M} and $\mathcal{R}(\mathbb{Q})$. Formally,

$$\begin{aligned} \mathbb{P}^{2n+1} &= \arg \min_{\mathbb{P} \in \mathcal{M}} \{ \text{KL}(\mathbb{P}^{2n} \parallel \mathbb{P}) \}, \\ \mathbb{P}^{2n+2} &= \mathbb{P}_{0,T}^{2n+1} \mathbb{Q}_{|0,T}. \end{aligned} \quad (13)$$

Given \mathbb{P}^{2n+1} , sampling from \mathbb{P}^{2n+2} can be done by first sampling from $\mathbb{P}_{0,T}^{2n+1}$, discarding intermediate steps, and then sampling from the diffusion bridge $\mathbb{Q}_{|0,T}$ by, for instance, Doob's h -transform. The first step can then be done under samples from \mathbb{P}^{2n+1} by techniques akin to score matching (see, Section A.1.1). Under weak conditions, it can be shown that the sequence \mathbb{P}^n converges to \mathbb{P}^{SB} as $n \rightarrow \infty$, and that it preserves the marginal distributions $\mathbb{P}_0^n = \pi_0$, $\mathbb{P}_T^n = \pi_T$ which is the key difference compared to the IPF approach.

A.2 Conditional generative models

In many applications, rather than unconditional sampling from a distribution $\pi(x)$, we are interested in generating conditional samples $\pi(x \mid y)$ for an observation y under a joint model $\pi(x, y)$. In this section, we review several conditioning methods for diffusion models, focusing on bridging.

A.2.1 Conditional score matching

Score-based generative models can readily generate conditional samples from pre-trained unconditional models by plugging $\nabla_x \log \pi(y \mid x)$ into the drift of (9). However, it is in general hard to know $\pi(y \mid x)$ or its score, for example, in image restoration/classification applications (Song et al., 2021). Due to this, one often needs to approximate a separate time-varying model for $\pi_t(y \mid x_t)$ or make domain-based heuristics, but this inevitably incurs additional errors for the conditional sampling.

A.2.2 Conditional Schrödinger bridges

Song et al. (2021) which requires learning or approximating the likelihood $\pi_t(y \mid x_t)$. By contrast, Shi et al. (2022) propose a method to learn a conditional sampler only requiring being able to sample artificial observations $\pi(y \mid x)$. The idea is built upon constructing a Schrödinger bridge (see Section A.1.2) for the augmented distribution $\pi(x, y)$, namely

$$\mathbb{P}^{\text{CSB}} = \arg \min_{\substack{\mathbb{P} \in \mathcal{P}(\mathcal{C}) \\ \mathbb{P}_0 = \pi(y|x)\pi(x) \\ \mathbb{P}_T = \pi_{\text{ref}}(x|y)\pi(y)}} \text{KL}(\mathbb{P} \parallel \mathbb{Q}) \quad (14)$$

with reference measure \mathbb{Q} given by the system of SDEs

$$dX_t = a(X_t) dt + dW_t, \quad dY_t = 0, \quad (15)$$

with initial distribution $X_0, Y_0 \sim \pi(x, y)$ and an arbitrary drift a . In Equation (14), $\pi_{\text{ref}}(y | x)$ refers to any informative approximation to $\pi(x | y)$ that is easy to sample from. We can then apply the methodology introduced in Section A.1.2 to solve Equation (14).

Importantly, under (14) one samples $\pi(y) = \int \pi(y, dx)$ by repeatedly sampling a data-point $X \sim \pi(x)$ and then generating $Y \sim \pi(y | X)$. This makes CSB ill-suited to problems for which one has only access to joint samples (X, Y) from the data, rather than to an observation-generator. Furthermore, CSB requires *training* a specialised conditional model, adding to the complexity and the approximate nature of the resulting conditional sampler.

A.3 Twisted diffusion samplers

When an observation model $p(y | x)$ is available, and given a discretised version of (5), it is possible to form an augmented model

$$U_{t_{k+1}} = U_{t_k} + f_{\text{rev}}(U_{t_k}, t_k)(t_k - t_{k-1}) + \epsilon_k, \quad U_0 \sim \pi_{\text{ref}}, \quad Y \sim \pi(y | U_T), \quad (16)$$

for which the conditional distribution of $U_T | y$ is $\pi(\cdot | y)$. This corresponds to a state-space model with a final observation $Y = y$, which can therefore be sampled by running the reverse diffusion (16) and then correcting the samples via importance sampling at the final time step. This is however well-known to be inefficient (Whiteley and Lee, 2014) as the unconditional samples U_T are unlikely to be distributed according to $\pi(\cdot | y_T)$.

In order to efficiently sample from $\pi(\cdot | y)$, Wu et al. (2023) proposed to form the twisted model

$$\tilde{U}_{t_{k+1}} \sim \tilde{p}(u_{t_{k+1}} | y, u_{t_k}), \quad \tilde{U}_0 \sim \pi_{\text{ref}} \quad (17)$$

enabling the following posterior distribution

$$\pi(U_{t_{0:K}} | y) = \pi_{\text{ref}}(U_0) \prod_{k=0}^{K-1} \tilde{p}(u_{t_{k+1}} | y, u_{t_k}) \frac{p(y | u_{t_{k+1}})p(u_{t_{k+1}} | u_{t_k})}{p(y | u_{t_{k+1}})\tilde{p}(u_{t_{k+1}} | y, u_{t_k})}, \quad (18)$$

which marginally recovers $\pi(U_T | y)$. Once an approximation $\tilde{p}(u_{t_{k+1}} | y, u_{t_k})$ to the true conditional process $p(u_{t_{k+1}} | y, u_{t_k})$ is chosen, the twisted model (17) can then be sampled from using particle filtering, with a proposal $\tilde{p}(u_{t_{k+1}} | y, u_{t_k})$ and the corresponding importance weights as given in (18), see also Wu et al. (2023); Whiteley and Lee (2014) for more details. While principled, this approach presents at least the following two issues: (i) it requires the likelihood model $\pi(y | x)$ to be known, which is not the case in most applications of interest, (ii) and it is computationally intensive as forming the approximation \tilde{p} requires the denoising score function to be differentiated (Wu et al., 2023, Section 3.2).

A.4 Pathwise conditioning

The idea of conditioning on the path of a diffusion process has been explored in the context of diffusion models by Trippe et al. (2023) for scaffolding and by Dou and Song (2024, concurrent with our paper) for the slightly more general setting of inverse problems. The idea is that, given an observation $Y = y$, and provided that the forward noising diffusion for X_t, Y_t is separable, one can form a sequence of observations $Y_{0:K}$ and then sample from the conditional distribution $\pi(X_{0:K} | Y_{0:K})$ by running the reverse diffusion (5) conditioned on $Y_{0:K}$ for instance by using a particle filter as in Wu et al. (2023). Beside the need for a separable noising SDE, the method is asymptotically consistent under three assumptions:

1. $p(X_T | y_0) \approx \pi_{\text{ref}}(X_T)$, that is, the forward noising process forgets the initial condition y_0 fast enough;
2. the number of particles N is large enough to ensure that the particle filter is sufficiently close to the true posterior;
3. the forward noising dynamics is separable.

Condition 1 is hard to verify in practice, condition 2 is computationally expensive to ensure, and condition 3 does not cover all useful models, therefore making the method impractical for many applications. Furthermore, once the reverse diffusion has been run, the samples only constitute an approximation to the conditional distribution, for a single observation path $Y_{t_0:K}$. Therefore the method needs to be repeated for another observation path $Y'_{0:K}$ if one wants an independent sample from $\pi(X_{0:K} | Y'_{0:K})$ and all intermediary samples need to be discarded accordingly. Nonetheless, as we explain in Section 5, this approach is a biased approximation of the PMMH algorithm we develop in Section 3.2 as it ignores the acceptance probability for the new path $Y'_{0:K}$.

B Experiment settings

In this section, we detail our experimental setting and report additional results supporting the conclusions of our experiments.

B.1 Common settings

Unless otherwise stated, our Gibbs-CSMC method applies the explicit backward sampling in Section 3.1 and the killing conditional resampling (Karppinen et al., 2023), and our PMCMC method applies the PCN proposal of Cotter et al. (2013) and stratified resampling (Chopin and Papaspiliopoulos, 2020, Chap. 9).

For image-related experiments, we use a standard UNet commonly used in denoising diffusion models (see Ho et al., 2020) with three downsampling and three upsampling layers, and we use the pixel shuffle method for upsampling in the UNet. The initial number of convolution features is 64, followed by 128, and 256 in the three layers. The detailed construction of the neural network is given in our companion code repository at <https://github.com/zgbkdlm/fbs>.

We randomly split the MNIST dataset into 60,000 training and 10,000 test data points. As for the CelebaHQ dataset (Liu et al., 2015), we split it into 29,000 training and 1,000 test data points. All the image data are normalised within the range $[0, 1]$.

All experiments are implemented in JAX (Bradbury et al., 2018) with the Flax (Heek et al., 2023) neural network backend. The experiments are conducted on an NVIDIA A100 80G GPU and the code required to reproduce our empirical findings can be found at <https://github.com/zgbkdlm/fbs>.

B.2 High-dimensional synthetic conditional sampling

In this experiment, our goal is to sample the posterior distribution of a Gaussian process model

$$\begin{aligned} f(\tau) &\sim \text{GP}(0, C(\tau, \tau')), \\ y(\tau) | f(\tau) &\sim \text{N}(0, \Xi), \end{aligned}$$

where C is an exponential covariance function with length scale $\ell = 1$ and magnitude $\sigma = 1$, and the observation noise covariance Ξ is a unit diagonal matrix. The GP regression is taken on 100 test points uniformly placed at $\tau \in [0, 5]$, resulting in a 100-dimensional target conditional distribution to sample from. The forward noising process is chosen to be $dX_t = -0.5 X_t dt + dW_t$ at $t \in [0, 1]$, so that we can compute the associated score function exactly by computing the marginal mean and covariance of X_t . For each single experiment and each method, we generate 10,000 conditional samples, and then repeat the experiment independently 100 times to report the results. To show how the samples approximate the true distribution, we compute the KL divergence, Bures–Wasserstein distance, and the mean absolute errors on the marginal means and variances.

While the CSGM method needs the likelihood distribution $p(y | x_t)$ to work (Song et al., 2021), in this Gaussian special case, the likelihood is analytically tractable, and hence the method can be applied exactly. For the twisted PF, we apply the GP observation model as the twisting function as per Wu et al. (2023, Eq. (8)).

Figure 5 compares the true and approximate distributions over two marginal random variables. The figure shows that the Gibbs-CSMC method outperforms others, followed by the PMCMC method. Increasing the number of particles gives noticeable improvements for the PF and TPF methods, meaning that these two methods require larger numbers of particles to work well for high-dimensional conditional samplings.

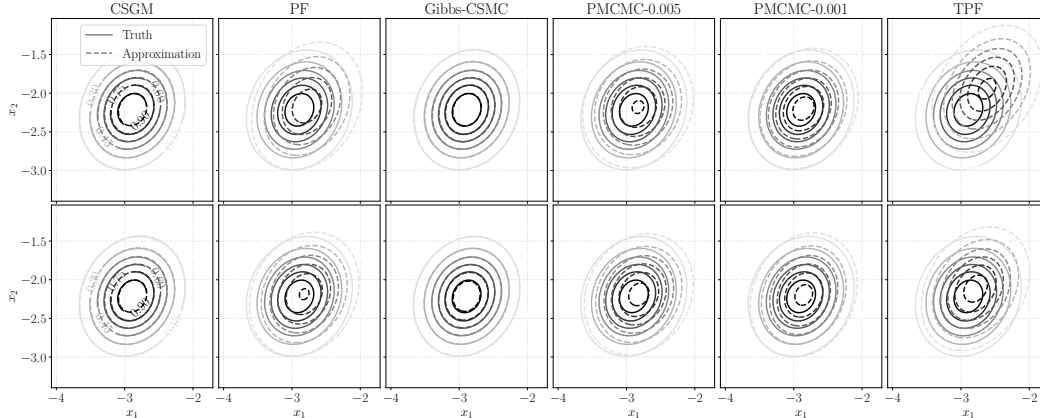


Figure 5: Contour plot of two-dimensional marginal densities for the true and approximate distributions in Section 4.1. The contour level lines are consistent in all the figures. The first and second rows show the results when using 10 and 100 particles, respectively. The figure shows that the Gibbs-CSMC method is visibly the best, and that it works well, even when using a small number of particles.

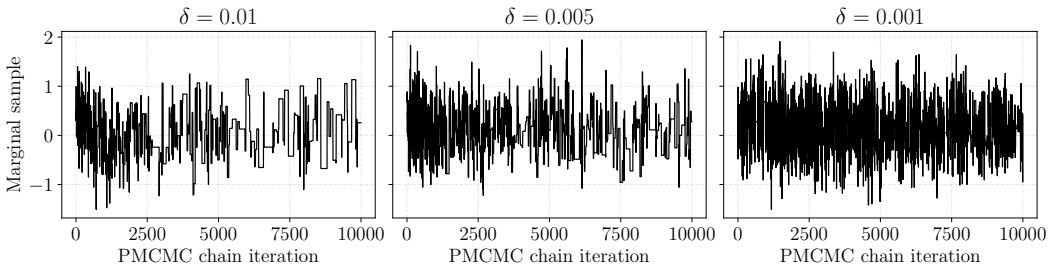


Figure 6: Trace plot of the PMCMC chain for the conditional sampling in Section 4.1 when using 10 particles and different δ . The traces are downsampled by 2 for visibility. We see that the calibration of δ reflects the effectiveness of the MCMC chain.

Figure 6 shows the trace of the PMCMC chain of one marginal variable. We see that the parameter δ affects the autocorrelation of the MCMC chain, which is also reflected in Table 1 and Figure 1. The chain appears to be more effective when δ is small, meaning that the measurement path $t \mapsto Y_t$ in Section 3.2 ideally should not move too much. Furthermore, we also see that the chain seems to gradually degenerate as the chain iteration goes for larger moves in the Y space. This is a well-known defect of pseudo-marginal methods (Andrieu and Roberts, 2009) in general, and comes from the fact that proposed paths are likely to be accepted originally due to the variance in the acceptance ratio, and then unlikely once the process has stabilised if the proposed path is too far from the current one. Solving this problem is an interesting avenue of future work and likely involves redesigning the proposal kernel for the path Y to take into account the specific structure of the model.

B.3 Conditional sampling in non-separable noising processes

In this section, we detail the experimental setting of Section 4.2.

To show the effect of using a non-separable noising process, we conduct quantitative and qualitative experiments using Schrödinger bridges. In the quantitative experiment, we apply the same GP model in Appendix B.2, but we scale the observation noise covariance to 0.1 to increase the correlation between X and Y . We use a Wishart distribution to randomly generate the reference covariance matrix $Q = q \otimes q$, where \otimes is the outer product, and $q \sim \mathcal{N}(0, I_d)$. We then consider a Gaussian Schrödinger bridge between $\pi(x, y)$ and $\mathcal{N}(0, Q)$, with reference process $dZ_t = dW_t$ given as the standard Brownian motion, the formulation of which is analytically tractable (Bunne et al., 2023).

For the qualitative experiments on MNIST images, we train a Schrödinger bridge with reference process $dZ_t = -0.5 \beta_t Z_t dt + \sqrt{\beta_t} dW_t$ at $t \in [0, 0.5]$, where $\beta_t := (b_{\max} - b_{\min}) / (T - t_0) t +$

$(b_{\min} T - b_{\max} t_0) / (T - t_0)$, and we set $b_{\max} = 5$, $b_{\min} = 0.02$, $t_0 = 0$, and $T = 0.5$. The reference distribution π_{ref} at T is a standard unit Gaussian. The number of Schrödinger bridge iterations is 20. At each Schrödinger bridge iteration, we run 20 epochs training the forward and backward models, with spatial batch size 64 and temporal batch size 32. We use the Adam (Kingma and Ba, 2015) optimiser with learning rate decaying from 2×10^{-4} to 2×10^{-6} in a cosine curve (Loshchilov and Hutter, 2017). For more details on the algorithm used to train the bridge, see De Bortoli et al. (2021, Algorithm 1).

Figure 7 shows additional examples of the MNIST super-resolution task using this Schrödinger bridge unconditional sampler model. In this figure, we reproduce the results returned by PF with various initialisations for X_0 and compare them to our Gibbs-CSMC method. Specifically, in PF we generate the initial value for X_0 using random uniform values (between 0 and 1), all zeros, and a linear interpolation based on y . This starting value is then used within the learnt non-separable noising diffusion to generate the measurement path is then used for the backward filtering routine. When using our CSMC-Gibbs method, we did not observe significant differences arising from the choice of the initial X_0 , and therefore report the result using an initial $X_0 = 0$ only.

As shown in Figure 7, the initialisation of X_0 indeed affects the quality of PF samples due to the non-separability of the Schrödinger bridge, while our Gibbs-CSMC sampler returns valid samples. This visible bias stems from the fact that, under non-separability, the choice of X_0 has a direct impact on the distribution of the path $Y_{1:K} | Y_0 = y, X_0$, as conditional independence is then not verified anymore. For the path $Y_{1:K} | \{Y_0 = y, X_0\}$ to be marginally distributed according to the forward noising diffusion (as required by Trippe et al., 2023), one would need the initial value of X_0 to be distributed according to $\pi(x | y)$, which is the problem we are trying to solve and is therefore not feasible in practice. While it is reasonable to assume that approximate samples from $\pi(x | y)$ can be obtained via other methods, this would incur additional computation and still not eliminate the bias. On the other hand, our Gibbs-CSMC method provides a natural way to produce samples that iteratively converge to $\pi(x | y)$, explaining its improved performance.

B.4 Image inpainting and super-resolution

In this section, we describe the image inpainting and super-resolution experiments of Section 4.3. These two tasks can be solved by our conditional samplers without dedicated training. Namely, given a corrupted image, we can obtain clean images by using our samplers as they are, on pre-trained generative diffusion models. More precisely, for any image $Z \sim \pi(dz)$, we split it into the unobserved X and observed Y parts, which correspondingly separate the (backward) generative diffusion of (7) for $\pi(dz)$. When the task is super-resolution, we model the observed low-resolution image as a subsampling of the original image. We then model the image inpainting and super-resolution as sampling from the unobserved pixels conditioned on the observed pixels.

For both tasks, we use a time-varying linear SDE as the noising process as in (7). Specifically, the forward process is given $dZ_t = -0.5 \beta_t Z_t dt + \sqrt{\beta_t} dW_t$ at $t \in [0, 2]$, where $Z_t := [X_t, Y_t]$, $\beta_t := (b_{\max} - b_{\min}) / (T - t_0) t + (b_{\min} T - b_{\max} t_0) / (T - t_0)$, and we set $b_{\max} = 5$, $b_{\min} = 0.02$, $t_0 = 0$, and $T = 2$.

We first pre-train the unconditional model to approximate the resulting score function using the standard denoising score matching method of Song et al. (2020). The optimiser we used for training is Adam with a decaying cosine learning rate schedule, i.e., the learning rate starts from 2×10^{-4} and ends at 2×10^{-6} following a cosine curve (Loshchilov and Hutter, 2017). The spatial and temporal batch sizes are 256. We also apply gradient clipping and exponential moving average (with 0.99 decay rate per two iterations) as suggested in Song and Ermon (2020). We run the training for 3,000 epochs and use the model obtained in the last epoch.

In the inpainting task, we apply rectangles of sizes 15 and 32 for MNIST and CelebAHQ, respectively, spawning at random locations (uniformly) in the image. As for super-resolution, we use rates 4 and 2 for MNIST and CelebAHQ. Precisely, rate 2 means that for an image of size 32 by 32, we partition it into 16 by 16 squares, where each square has 2 by 2 pixels; at each square, we randomly select one pixel for the low-resolution image. For each test (inpainting/super-resolution) image, we generate 100 restored image samples, and report the statistics as in Tables 2 and 3. In the table, the LPIPS score uses an Alex net (Zhang et al., 2018). The commonly used Fréchet inception distance is not

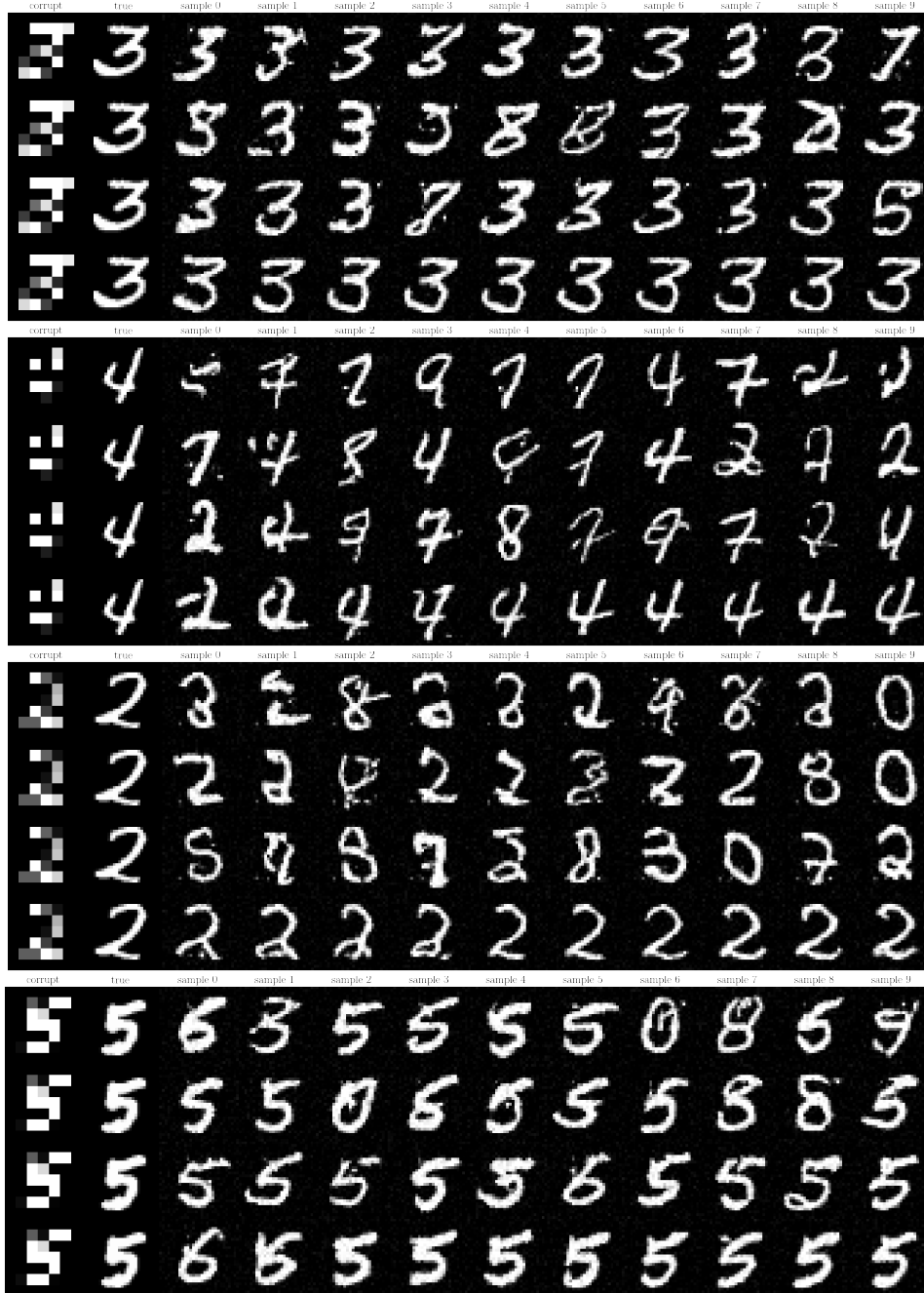


Figure 7: MNIST super-resolution (x4) on a Schrödinger bridge. The four panels illustrate four test samples. In each panel, the first to last rows show the samples of PF (using random initialisation), PF (using all-zeros initialisation), PF (using linear interpolation initialisation), and our Gibbs-CSMC method, respectively. The initialisation in PF affects the quality, with the linear interpolation slightly better than other initialisations. Nonetheless, all PF methods generate worse samples compared to Gibbs-CSMC. For Gibbs-CSMC, while the initial sample is poor, it gradually improves and reaches the ‘true’ stationary distribution $\pi(x | y)$ in a few iterations of the MCMC chain.

applied here, since it is not clear how to use it to benchmark MCMC samples (cf. the arguments in Cardoso et al., 2024).

For the CSGM method, we implement the conditional drift as per Song et al. (2021, Sec. I.2). As for the TPF, we also implement the same twisting function as in Wu et al. (2023, Sec. 3.3).

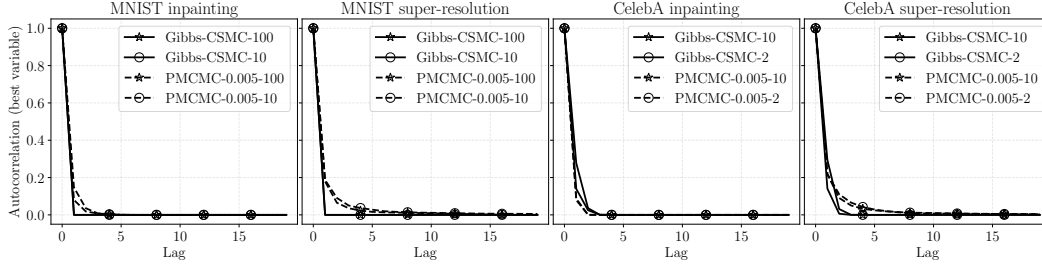


Figure 8: Autocorrelations of Gibbs-CSMC and PMCMC (with $\delta = 0.005$) for image inpainting and super-resolution. The autorrelations are averaged over 100 individual test samples. For each test sample, its autocorrelation is computed over 100 MCMC samples, and we select the best curve among all the image pixels. We select the best curve because some pixels will not change at all given the problem definition. The autocorrelation of Gibbs-CSMC is marginally better than PMCMC.

We show samples of inpainting and super-resolution tasks in Figures 9–12, to qualitatively compare the methods. We find from these figures that our Gibbs-CSMC and PMCMC methods indeed outperform all other methods, in terms of quality and correctness. By correctness, we mean that the samples generated by our methods are realistic and closer to the true images. As an example, in the first panel of Figure 9, the MCMC chains generate a variety of digits “4” which indeed correspond to the true digit, while other methods can generate wrong, albeit more diverse digits.

The autocorrelations of Gibbs-CSMC and PMCMC methods are shown in Figure 8. We see that both MCMC methods admit reasonable autocorrelations in all the tasks, while Gibbs-CSMC is better than PMCMC.

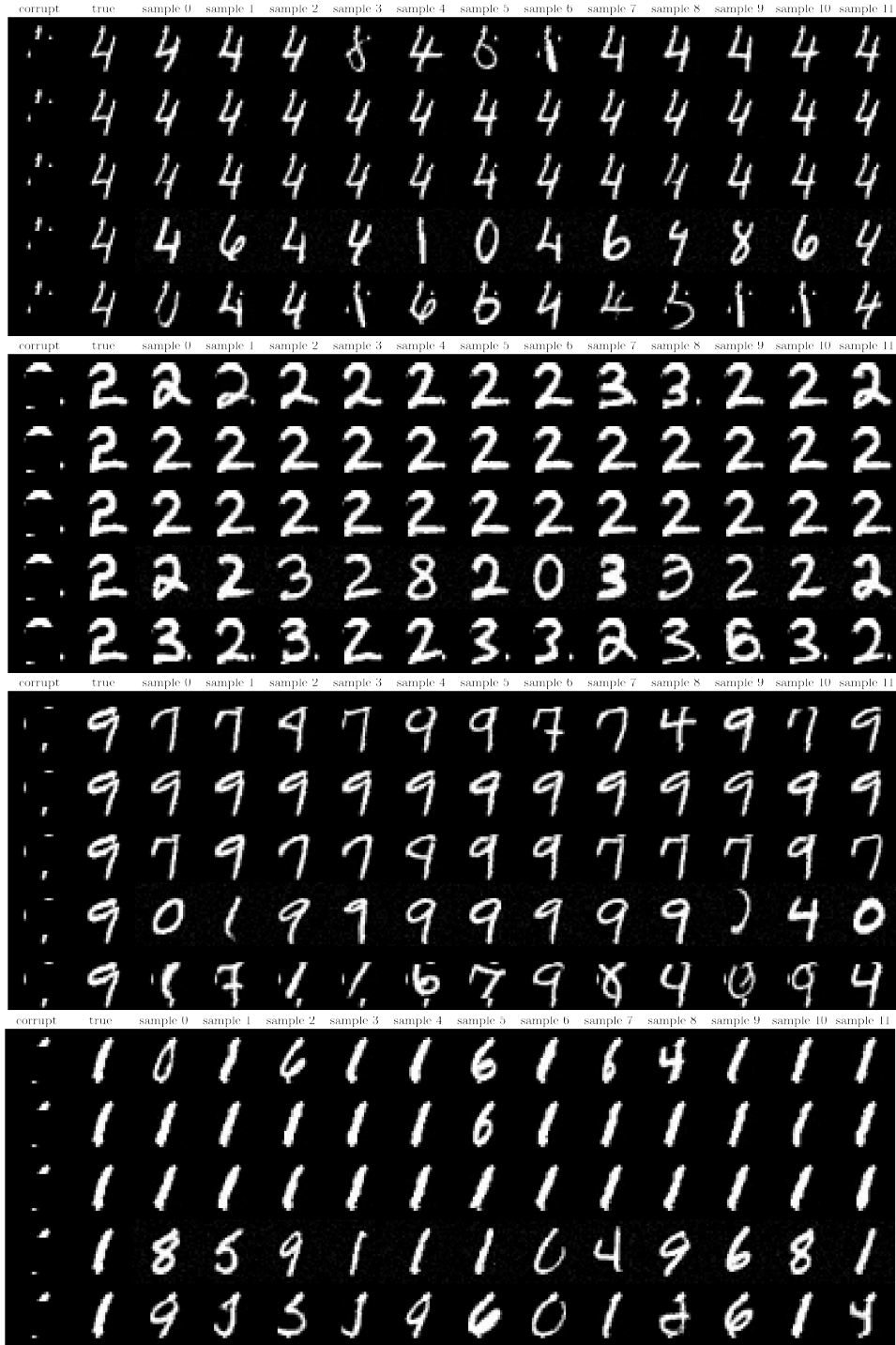


Figure 9: Examples of MNIST inpainting (using 100 particles) tasks. The figure has four panels, showing the results for four test images. In each panel, the first to last rows show the results of PF, Gibbs-CSMC, PMCMC-0.005, TPF, and CSGM, respectively. Wrong samples and artefacts appear less in our MCMC methods compared to others.

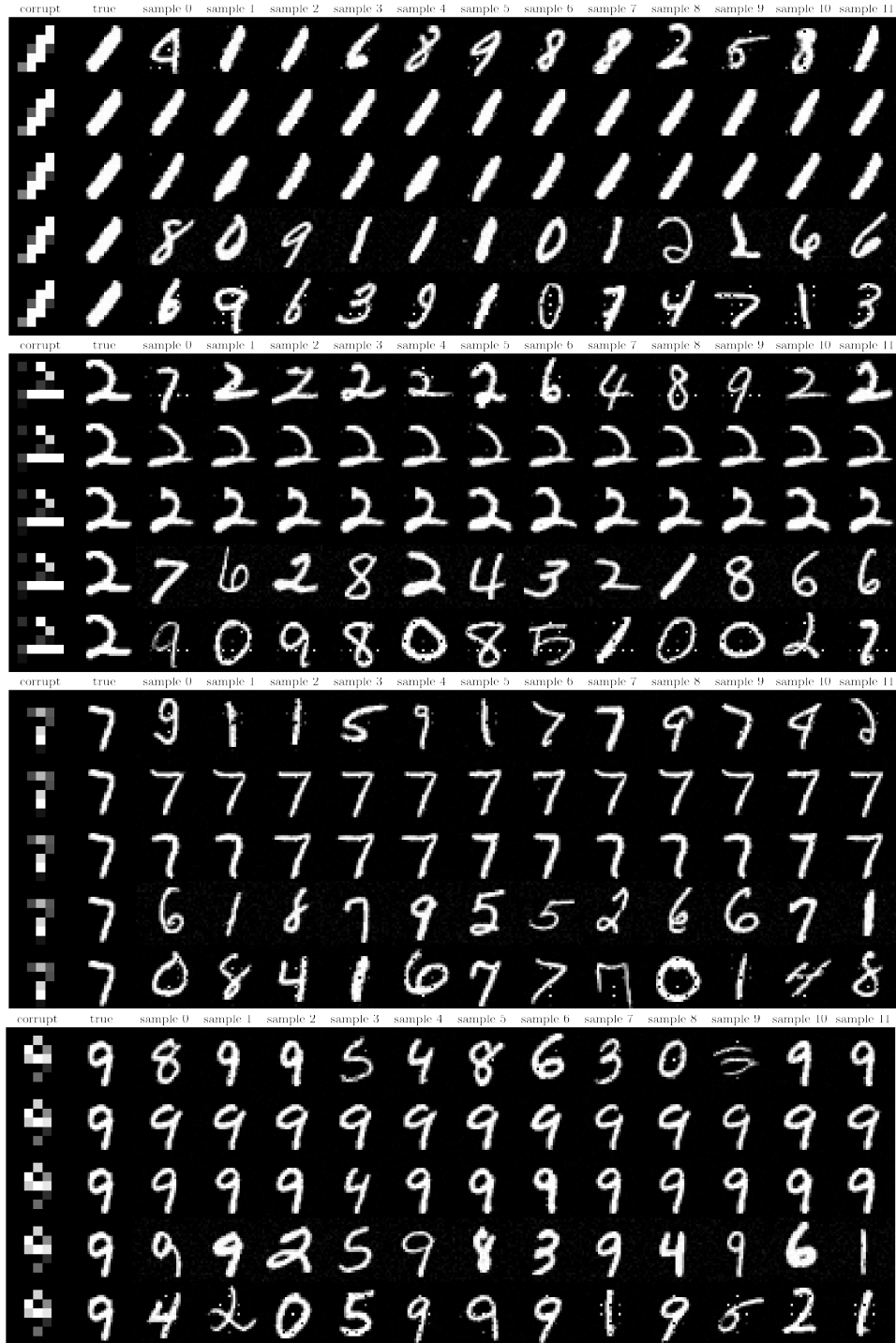


Figure 10: Examples of MNIST super-resolution tasks. The figure has four panels, showing the results for four test images. For each panel, the first to last rows show the results of PF, Gibbs-CSMC, PMCMC-0.005, TPF, and CSGM, respectively. Wrong samples and artefacts appear less in our MCMC methods compared to others.

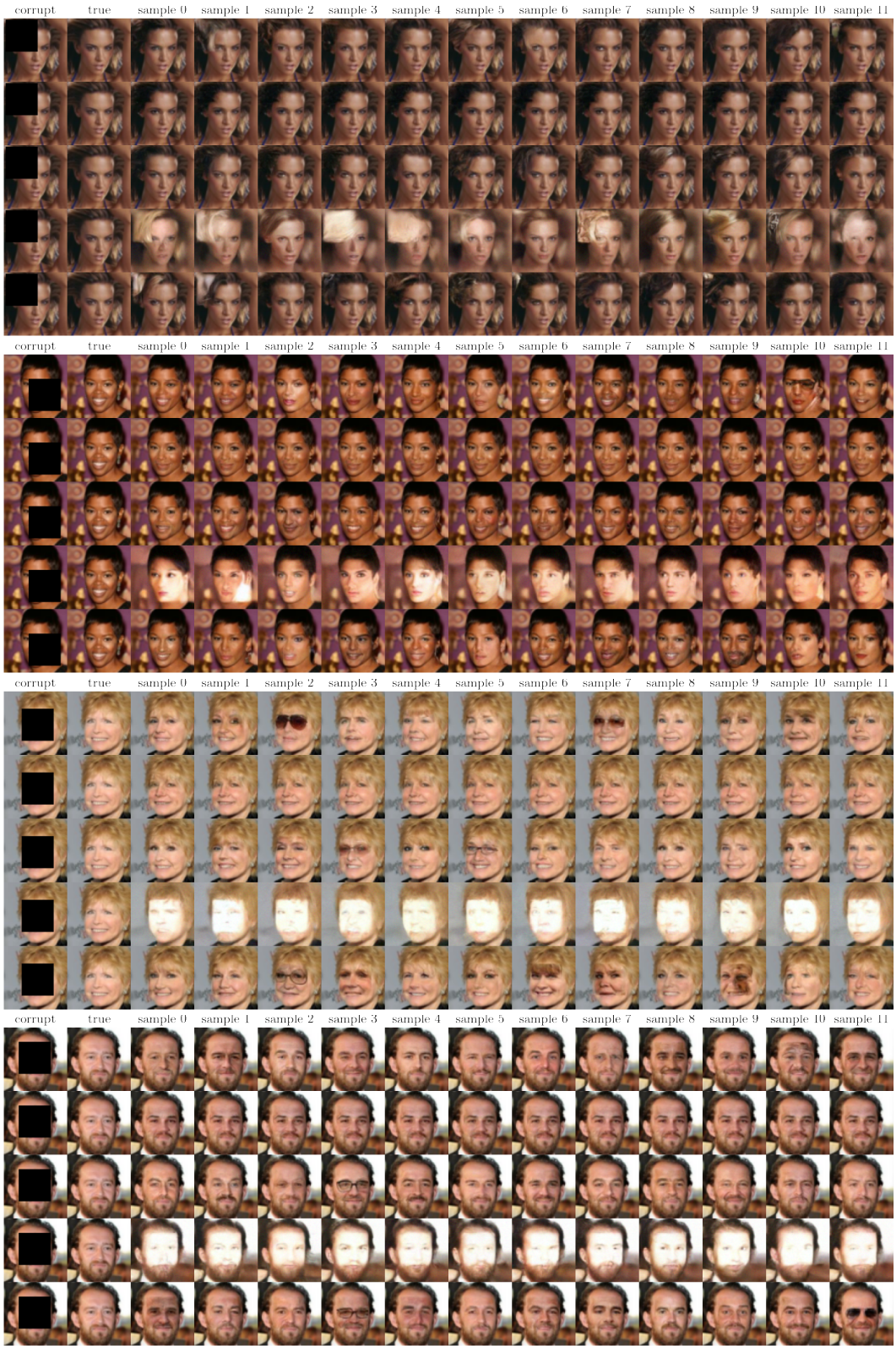


Figure 11: Examples of CelebAHQ inpainting tasks. The figure has four panels, showing the results for four test images. For each panel, the first to the last rows show the results of PF, Gibbs-CSMC, PMCMC-0.005, TPF, and CSGM, respectively.

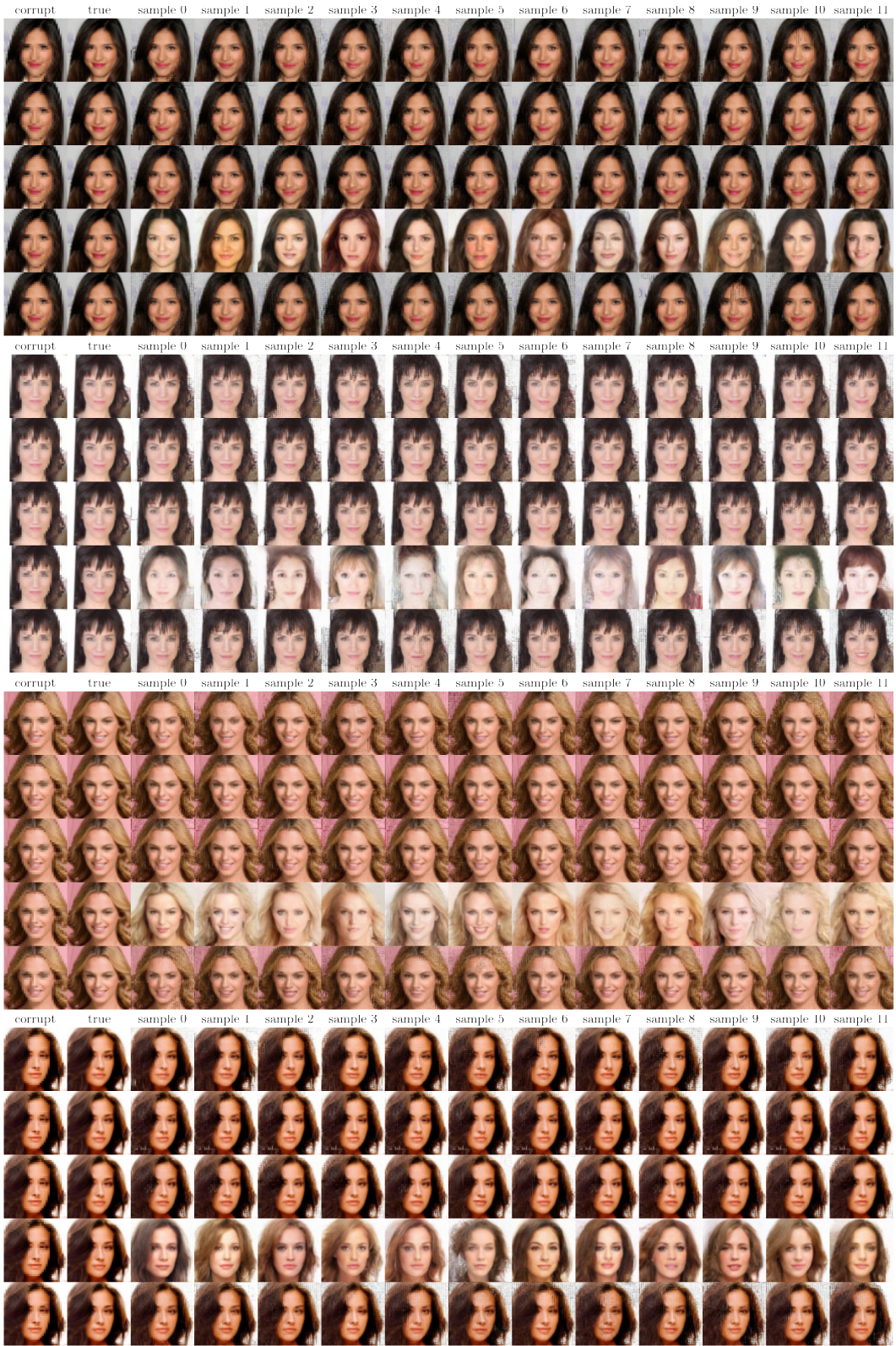


Figure 12: Examples of CelebA super-resolution tasks. The figure has four panels, showing the results for four test images. For each panel, the first to the last rows show the results of PF, Gibbs-CSMC, PMCMC-0.005, TPF, and CSGM, respectively.